Wind-driven lateral variations of partial pressure of carbon dioxide in a large estuary

Wei-Jen Huang[1,2*], Wei-Jun Cai[2], Xiaohui Xie[3], Ming Li[3]

[1] Department of Oceanography, National Sun Yat-sen University, Kaohsiung, Taiwan

[2] School of Marine Science and Policy, University of Delaware, Newark, DE 19716, USA

[3] Horn Point Laboratory, University of Maryland Center for Environmental Science, P.O. Box 775, Cambridge, MD 21613, USA

Corresponding author: Wei-Jen Huang (wjhuang29@mail.nsysu.edu.tw)

Key words: carbon cycle; hypoxia; carbon dioxide; cross-channel; vertical variation

Declarations of interest: none

Abstract

Estuarine carbon cycle and biogeochemical studies usually focus on along-estuary variations and neglect cross-estuary variations. In a stratified middle reach of the Chesapeake Bay, we observed a counterclockwise circulation and upwelling of subsurface water with high partial pressure of carbon dioxide ($p\mathrm{CO_2}$) on the eastern shoal during a down-estuary wind event from October 24 to 25, 2013. The average air-sea CO_2 gas exchange flux over the eastern one-third of this cross transect was approximately 20 to 40% higher, while the flux over the western 1/3 was lower by a similar amount, compared with the middle section. A statistically strong correlation between $p\mathrm{CO_2}$ and salinity values was observed, suggesting the presence of a high CO_2 source from the higher salinity bottom water. The observations suggest that wind-driven lateral upwelling can enhance the release of respired CO_2 from subsurface water in stratified large estuaries by as much as 30% over a short time-scale of hours.

1 Introduction

Globally, estuaries and bays cover an area that is only 0.03% of the total area of open oceans, but they remain an important part of the carbon cycle among land, ocean, and atmosphere [*Raymond et al.*, 2000; *Zhai et al.*, 2005; *Hunt et al.*, 2014; *Borges et al.*, 2015; *Joesoef et al.*, 2015]. Most estuaries act as a source of carbon dioxide (CO_2) for the atmosphere [*Borges et al.*, 2006; *Chen and Borges*, 2009], returning a large part of the CO_2 taken up by the land back to the atmosphere as carbon that is transported to the ocean along the land-ocean continuum. In contrast, continental shelves and open oceans are CO_2 sinks [*Chen and Borges*, 2009; *Bauer et al.*, 2013]. The Chesapeake Bay, known for its autotrophic status due to anthropogenic nutrient input, is a good study site that is representative of eutrophic estuaries on the U.S. east coast and elsewhere.

The partial pressure of CO_2 (pCO_2) is usually measured along the main axis of an estuary to capture the variations in air-sea CO_2 fluxes across the longitudinal salinity gradient between its riverine and oceanic boundaries [*Raymond et al.*, 2000; *Zhai et al.*, 2005; *Hunt et al.*, 2014; *Borges et al.*, 2015; *Joesoef et al.*, 2015]. Meanwhile, variations in CO_2 fluxes in the cross-channel direction are often neglected. However, strong lateral gradients in salinity, dissolved oxygen, and nutrient concentrations have been reported in previous observations [*Boicourt*, 1992; *Lacy et al.*, 2003; *Aristizábal and Chant*, 2014]. In a similar vein, a lateral gradient and lateral circulation could significantly affect the CO_2 fluxes over estuaries, but little is known about these effects. The cross-channel pCO_2 variations can further lead to spatial uncertainties in estimating air-sea CO_2 fluxes over estuaries.

A riverine nutrient flux fuels a spring phytoplankton bloom from April to mid-May in the Chesapeake Bay [*Malone*, 1992]. Organic materials derived from sinking phytoplankton provide the substrate to support a robust microbial community, whose metabolic activities draws down dissolved oxygen to the hypoxic level (dissolved oxygen < 2 mg L^{-1}) in the near-bottom water [*Kemp et al.*, 1992, 2005; *Hagy et al.*, 2004]. Hypoxia has been shown to be a source of dissolved inorganic carbon (DIC) and pCO_2 [*Cai et al.*, 2017; *Hu et al.*, 2017]. Vertical mixing due to storms or the seasonal evolution of the surface mixed layer may facilitate the release of bottom DIC, as shown in other coastal oceans [*Cai et al.*, 2011; *Chou et al.*, 2011]. Other physical mechanisms, such as wind-driven lateral upwelling, could also promote bottom DIC release in a stratified estuary.

Wind-driven upwelling has been shown to affect biogeochemical cycling on continental shelves [*Anderson et al.*, 2009; *Lachkar*, 2014]. Along-channel winds can also generate lateral Ekman flows and isopycnal movements in estuaries, leading to the upwelling or downwelling of bottom water and providing a potential pathway for nutrients and dissolved oxygen [*Malone et al.*, 1986; *Sanford et al.*, 1990; *Wilson et al.*, 2008; *Scully*, 2010; *Li and Li*, 2012; *Xie et al.*, 2017c]. In a modeling study of Chesapeake Bay, *Scully* [2010] showed that the wind-driven lateral exchange between the deep-channel and shallow shoals may be more important than vertical mixing in ventilating the hypoxic bottom water. However, it remains unclear how this wind-driven upwelling mechanism affects CO_2 dynamics. In particular, there have been very few measurements of CO_2 in the Chesapeake Bay.

With a rich record of physical and biogeochemical data, the Chesapeake Bay provides an ideal site to study the effects of physical processes on lateral variations in pCO$_2$ and the impact on air-sea CO_2 fluxes in large estuaries. This study reports repeated measurements of pCO$_2$ at a cross-channel section in the middle of the Chesapeake Bay. Five moorings spanned a cross-channel section in the mid-bay and provided continuous measurements of temperature, salinity and currents. To the extent of our knowledge, this is the first study to measure *in situ* physical quantities and pCO$_2$ together across a stratified estuarine channel and interpret surface pCO$_2$ variations in the context of physical processes. Factors controlling pCO$_2$ are discussed, and a conceptual model is presented to summarize the effects of wind driven lateral circulation on pCO$_2$ variations in the estuary.

2 Data and Methods

We surveyed a small rectangular area (6 km and 1.2 km along the cross-channel and along-channel directions, respectively) in the middle of Chesapeake Bay on board the *R/V Sharp* (Fig. 1a), surrounding a line of moorings that had been deployed to measure physical properties [*Fisher et al.*, 2015; *Scully*, 2016; *Xie et al.*, 2017a, 2017b, 2017c]. The ship made 10 repeated surveys over a period of 16 hours on October 24-25, 2013 (hereafter we use D1 to D10 to represent each survey). The vessel completed each circuit in ~90 minutes with an average speed of 5 knots. Surface-water temperature, salinity, and pCO_2 were sampled via the ship's pumping system with an inlet from ~1 m depth. Atmospheric pCO_2 was sampled on top of the bridge of this ship. The value of pCO_2 was measured by a flow-through system with a CO_2 analyzer (LI-COR® 7000) (details described by *Jiang et al.*, [2008] and *Huang et al.*, [2015]). This pCO_2 system repeatedly measured 120 water samples after 10 air samples. The CO_2 analyzer was calibrated by using four certified gas standards (197.45, 400.57, 594.65, and 975.26 ppm) every 3.5 to 6 hours. These certified gas standards were referenced against standards traceable to the National Institute of Standards and Technology. As a result, we collected a total of 409 water pCO_2 samples during these 10 surveys (26.9 ± 7.8 samples per hour, 40.9 samples per survey), with a special resolution of 0.00371°. The average atmospheric pCO_2 value was 400.9 ± 2.1 μatm during the observational period. To better study fine-scale variabilities, we noticed a time lag between the recorded locations and the water sampling locations. This lag was ~0 to 3.7 minutes, depending on the ship speed and pCO_2 analysis time. Details can be found in SI and Fig. S1.

The vessel was equipped with a towed undulating vehicle (Scanfish). The Scanfish measured temperature and salinity every 0.5 seconds when it moved along the slanted path up and down the water column (with inclination angles approximately 6°). Five moorings were deployed in the cross-channel transect and were equipped with acoustic Doppler current profilers (bottom-mounted) and CTDs (conductivity, temperature, and pressure) (Sea-Bird MicroCat), providing continuous measurements of current velocity and temperature or salinity from 22 August to 31 October 2013 [*Xie et al.*, 2017a]. Wind speed was measured at a surface buoy on top of two of the five moorings. To examine the effects of lateral circulation and upwelling on pCO_2, velocities were rotated into the along-estuary (x) and across-estuary (y) components (u, v); that is, positive x and y directions are 340º N and 250º N (clockwise from the true north), according to the major axis of the depth-averaged tidal flows [*Xie et al*., 2017b].

We used the following equation [*Wanninkhof*, 1992] to calculate the air-sea CO_2 flux:

$$CO_2\ \mathrm{Flux} = k \times K_0 \times (pCO_{2sw} - pCO_{2air}), \quad (1)$$

where k is the gas transfer parameter, K_0 represents the solubility of CO_2 [*Weiss*, 1974]; and pCO_{2sw} and pCO_{2air} are the pCO_2 values in the near-surface water and in the air, respectively.

The air-sea gas transfer parameter was calculated by the equation given by *Ho et al.* [2006]. A small thermal effect caused by the difference in temperature between the shipboard pCO_2 equilibrator and the outside bay water was corrected using a method from *Takahashi et al.* [2002]. Details in the calculation of air-sea CO_2 flux can be found in *Huang et al.* [2015].

3 Results

During the ship survey period, down-estuary winds (northerly winds) blew down the estuary. Wind speed increased from D1 to D4 (setup phase), reached a maximum speed of 8-9 m s^{-1} at D5 to D6 (maximum phase), and decreased from D7 to D10 (set-down phases) (Fig. 1b). In the surface layer (0 to ~15 m deep), a counterclockwise lateral circulation developed on a vertical section at D1 (Fig. 1c), and tilted isopycnals developed upwards along the eastern shoal, resulting in the upwelling of subsurface water that started at D3 (Fig. 1d). At the peak wind speed (D5), the upwelled high-salinity water spread westward over the deep channel (Fig. 1e) and produced a lateral salinity difference of ~0.7 psu between the eastern and western shoals. During the set-down phase (D10), the lateral circulation weakened and displayed a complex vertical structure [*Xie et al.,* 2017a], and the upwelling region retreated to the eastern shoal (Fig. 1f). On average, a salinity difference of ~0.3 psu between the eastern and western shoals was observed. In contrast, in the bottom boundary layer (~15 to 23 m deep), a clockwise circulation was observed and was driven by lateral Ekman forcing (Fig. 1c-f; Xie *et al*. 2017a). Through this wind event, surface temperature and salinities displayed strong cross-channel gradients, as confirmed by the measurements from the ship-board pumping system (Fig. 1g, h). To facilitate discussion, we separated this cross channel section into three segments. Water on the eastern one-third (1/3) segment had lower temperature and higher salinity (T: 16.50 ± 0.63°C; S: 16.38 ± 0.40 psu) than those in the western 1/3 segment (17.66 ± 0.36°C; 16.05 ± 0.08 psu).

The surface pCO_2 distributions displayed striking lateral gradients, with relatively higher pCO_2 values on the eastern shoal (490.3 ± 38.1 μatm) and lower values on the western shoal (453.5 ± 10.1 μatm) (Fig. 1i) (the pCO_2 spatial distribution in each circuit survey is presented in Fig. 2). This lateral pCO_2 gradient varied during the set-up, peak, and set-down phases of the wind-driven event. In the beginning (D1), the pCO_2 values were generally below 475 μatm, with a few values above 500 µatm right next to the eastern shoal. At the peak wind speed (D5), the eastern shoal was covered by $p$$CO_2$ values higher than 500 µatm (Fig. 1i). Finally, when the upwelling weakened during the set-down phase (D10 for example), the $p$$CO_2$ values were all below 500 µatm (Fig. 1i). Overall, $p$$CO_2$ values on the eastern shoal were still 5% higher than those in the middle segment, while $p$$CO_2$ values on the western shoal were 2% lower than those in the middle segment (Table 1). The $p$$CO_2$ values on the western shoal were significantly different from the values on the eastern shoal (two tailed t-test, $p < 0.001$). Particularly, the changes in $p$$CO_2$ values between shoals and the middle segment were enlarged during D5, that is, 5% to 9% on the eastern shoal and -2% to -6% on the western shoal (Table 1).

During the cruise period (late October), the mid-Chesapeake Bay acted as a CO_2 source to the atmosphere (average CO_2 flux of 10.26 ± 6.6 mmol m^{-2} d^{-1}), since the average surface water $p$$CO_2$ (467.1 µatm) was oversaturated with respect to the average atmospheric value (400.9 µatm) (Fig. 1j). The CO_2 flux also displayed strong lateral variations, ranging from 13.3 ± 5.8 mmol m^{-2} d^{-1} over the eastern segment of the estuary to 7.6 ± 1.6 mmol m^{-2} d^{-1} on the western shoal (Table 1). The air-sea CO_2 fluxes between these two shoals were significantly different from each other (two-tailed t-test, $p < 0.001$). During D5, CO_2 fluxes on the eastern shoal were 53% higher than values on the middle of the bay, whereas CO_2 fluxes on the western shoal were 46% lower (Table 1). Air-sea CO_2 fluxes on these two shoals during D5 were significantly different from each other (two-tailed t-test, $p < 0.001$). In addition, the CO_2 flux at the peak wind (D5) was 27% higher than the average from the set-up (D1) to set-down (D10) phases (Table 1).

A time lag between the recorded locations and the sampling locations was observed and varied slightly from ~0 to 3.7 minutes over the entire study. We systematically reconciled this variable time lag by binning all data into the western shoal, middle, and eastern shoal for this study. When this lag time was near a constant value of ~3.7 minutes during D5, its effect on the variation in $p$$CO_2$ and CO_2 flux was observed in the middle segment of the bay (Fig. 1i,j) and can be reconciled by simply removing this time lag (details in SI, Fig. S1).

The biogeochemical variables were highly correlated with the physical variables. During the three phases of the wind event, both bin-averaged $p$$CO_2$ and CO_2 fluxes (for each survey) were statistically correlated with the bin-averaged salinity, respectively (R^2 = 0.89, 0.89, respectively) (Fig. 3a). This $p$$CO_2$ to salinity correlation (Fig. 3a) showed that the bin-averaged surface salinity at D5 was close to the salinity at 7 m depth at D1 (see Fig. 1). The above analysis implies that the wind-induced counterclockwise circulation replaced the surface pCO_2 on the eastern shoal with subsurface ones, thereby affecting the surface air-sea CO_2 flux over this estuary.

4 Discussion

4.1 CO_2 dynamics resulting from the counterclockwise circulation

The near-bottom water, with its strong net respiration, is a CO_2 source with a high DIC concentration [*Kemp et al.*, 2005; *Cai et al.*, 2017] and may serve as a biological end-member in addition to the river and sea water end-members. Assuming a conservative mixing of DIC and TA between the riverine and oceanic ends of the Chesapeake Bay produces a relationship between pCO_2 and salinity, as shown in Fig. 4. Our observed pCO_2 values in the mid-bay exceeded pCO_2 predicted from conservative mixing in this salinity class. The strong correlation between pCO_2 and salinity suggests that the cross-channel variation in pCO_2 was caused by the wind-driven counterclockwise circulation with upwelling on the eastern shoal of the estuary. Although we only had a detailed observation of one down-estuary wind event during this ship-of-opportunity cruise, previous observations and modeling studies show that these northerly winds have frequently impacted the Chesapeake Bay [*Sanford et al*., 1990; *Xie et al*., 2017c; *Xie and Li*, 2018]. Similar cross-channel variations in surface pCO_2 are expected under the up-estuary (southerly) winds. The up-estuary winds would drive a vertically clockwise circulation (in the surface layer) and cause upwelling on the western shoal [*Malone et al*., 1986; *Scully*, 2010; *Li and Li*, 2012; *Xie et al*., 2017c].

Phytoplankton biomass and net primary production (PP) were shown to exhibit large gradients in the cross-channel direction [*Lee et al.,* 2013; *Son et al.,* 2014], implying a PP-induced cross-estuary biological CO_2 uptake during daytime. This study was designed to minimize the effects of diel variation on water pCO_2 by conducting the surveys mostly after sunset (sunset was 18:14 on Oct. 24 and sunrise was 7:26 Oct. 25 at Annapolis, Maryland, https://www.timeanddate.com/sun/usa). Our pCO_2 data were mostly collected during the dark hours and were statistically related to salinity (Fig. 3a). Therefore, the possibility that observed cross-estuary pCO_2 variations were affected by PP variability during our sampling period was minimal.

Wind speed is known to be a critical factor in determining the air-sea CO_2 gas exchange rate [*Ho et al.,* 2006 and references therein] and, furthermore, is likely related to the surface pCO_2 distribution in this event. A positive correlation was observed between pCO_2 and wind speed, with an average R^2 value of 0.45 (Fig. 3b), and this correlation is weaker than the strong correlation observed between pCO_2 and salinity, suggesting that factors other than the wind speed may affect salinity [*Xie and Li*, 2018] and pCO_2. For example, *Xie et al.* [2017a] have shown that baroclinic effects are also important to wind-driven lateral circulation. Furthermore, we observed that the correlation was stronger during the set-up phase than during the set-down phase of this event (Fig. 3b). The observed surface pCO_2 signal could also have been compensated by the air-sea CO_2 gas exchange once the subsurface water was upwelled to the surface, but such gas exchange rate was not fast enough in releasing the accumulated DIC concentration in the water (that is, gas exchange generally has a time scale of a month or longer [*Cai et al.*, 2017]).

The difference in temperature between the two sides of the bay was approximately 2°C in this study (Fig. 1g) and would theoretically have resulted in a difference of approximately 20 µatm in pCO_2 (TA = 2400 µmol kg^{-1}, DIC = 2260 µmol kg^{-1}, T=16°C or 18°C). However, most of our measurements deviated beyond this expected relationship between temperature and pCO_2 (Fig. 5), suggesting that such temperature variations were not sufficiently strong to alter the pCO_2 distribution.

The upwelled water led to higher pCO_2 and air-sea CO_2 fluxes on the eastern shoal than on the western shoal. Therefore, wind-driven upwelling of high pCO_2 and acidified waters on shallow shoals may be a general phenomenon in the Chesapeake Bay and perhaps in other large estuaries too.

4.2 Synthesis and a conceptual model

A conceptual model is proposed to explain the observed cross-channel variations in surface pCO_2 during wind events (Fig. 6). We envision similar responses between the down-estuary and up-estuary wind events. The net heterotrophic subsurface water [*Kemp et al.*, 2005; *Testa and Kemp*, 2008; *Scully*, 2010] can be characterized by high DIC and low pH values [*Cai et al.*, 2017], and part of this water can be upwelled to the eastern shoal by the counterclockwise circulation under the down-estuary winds (or to the western shoal by the clockwise circulation under the up-estuary winds). Higher pCO_2 values could be found on one side of the estuarine cross section, resulting in a cross-channel gradient. Hence, wind-driven lateral upwelling (other than diffusion) can be a mechanism for releasing respired DIC in a stratified estuary. When anoxic conditions are observed in the stratified water column [*Cai et al.*, 2017], the most acidified water is typically located in the middle depths between the oxic and anoxic layers. The upwelling of this acidified water to the surface could significantly change the surface distribution of pCO_2 and thus, the air-sea CO_2 fluxes.

Acknowledgements: We are grateful for the financial support from NOAA (NA15NOS4780184 To ML) and NSF (OCE-1061609 to ML). WJC acknowledges support from the University of Delaware and from NOAA (NA15NOS4780190) on this study. The underway pCO_2 and related data are presented in Table S2 in SI. Acoustic Doppler current profilers and seabird MicroCat CTDs data set can be downloaded from the following link https://data.mendeley.com/datasets/xfjynnstxy/draft?a=a3d68e35-4756-4998-9833-9a8f5f7aabf9

References

Anderson, R. F., S. Ali, L. I. Bradtmiller, S. H. H. Nielsen, M. Q. Fleisher, B. E. Anderson, and L. H. Burckle (2009), Wind-driven upwelling in the Southern Ocean and the deglacial rise in atmospheric CO_2, *Science*, *323*(5920), 1443–1448, doi:10.1126/science.1167441.

Aristizábal, M., and R. Chant (2014), Mechanisms driving stratification in Delaware Bay estuary, *Ocean Dyn.*, *64*(11), 1615–1629, doi:10.1007/s10236-014-0770-1.

Bauer, J. E., W.-J. Cai, P. A. Raymond, T. S. Bianchi, C. S. Hopkinson, and P. A. G. Regnier (2013), The changing carbon cycle of the coastal ocean., *Nature*, *504*(7478), 61–70, doi:10.1038/nature12857.

Boicourt, W. C. (1992), Influences of circulation processes on dissolved oxygen in the Chesapeake Bay, in *Oxygen dynamics in Chesapeake Bay: A synthesis of research*, edited by D. Smith, M. Leffler, and G. Mackiernan, pp. 7–59, University of Maryland Sea Grant College, College Park, Maryland.

Borges, A.V, L. S. Schiettecatte, G. Abril, B. Delille, and F. Gazeau (2006), Carbon dioxide in European coastal waters, *Estuar. Coast. Shelf Sci.*, *70*(3), 375–387.

Borges, A.V., G. Abril, F. Darchambeau, C. R. Teodoru, J. Deborde, L. O. Vidal, T. Lambert, and S. Bouillon (2015), Divergent biophysical controls of aquatic CO_2 and CH_4 in the world's two largest rivers, *Sci. Rep.*, *5*, 15614, doi:10.1038/srep15614.

Chen, C.-T. A., and A.V Borges (2009), Reconciling opposing views on carbon cycling in the coastal ocean: Continental shelves as sinks and near-shore ecosystems as sources of atmospheric CO_2, *Deep Sea Res. Part II Top. Stud. Oceanogr.*, *56*(8–10), 578–590.

Cai, W.-J. et al. (2011), Acidification of subsurface coastal waters enhanced by eutrophication, *Nat. Geosci.*, *4*(11), 766–770, doi:10.1038/ngeo1297.

Cai, W.-J. et al. (2017), Redox reactions and weak buffering capacity lead to acidification in the Chesapeake Bay, *Nat. Commun.*, *8*(1), 369, doi:10.1038/s41467-017-00417-7.

Chou, W.-C., G.-C. Gong, C.-M. Tseng, D. D. Sheu, C.-C. Hung, L.-P. Chang, and L.-W. Wang (2011), The carbonate system in the East China Sea in winter, *Mar. Chem.*, *123*(1–4), 44–55, doi:10.1016/j.marchem.2010.09.004.

Fisher, A. W., L. P. Sanford, S. E. Suttles, A. W. Fisher, L. P. Sanford, and S. E. Suttles (2015), Wind stress dynamics in Chesapeake Bay: Spatiotemporal variability and wave dependence in a fetch-limited Environment*, *J. Phys. Oceanogr.*, *45*(10), 2679–2696, doi:10.1175/JPO-D-15-0004.1.

Hagy, J. D., W. R. Boynton, C. W. Keefe, and K. V. Wood (2004), Hypoxia in Chesapeake Bay, 1950-2001: Long-term change in relation to nutrient loading and river flow, *Estuaries*, *27*(4), 634–658, doi:10.1007/BF02907650.

Ho, D. T., C. S. Law, M. J. Smith, P. Schlosser, M. Harvey, and P. Hill (2006), Measurements of air-sea gas exchange at high wind speeds in the Southern Ocean: Implications for global parameterizations, *Geophys. Res. Lett.*, *33*(16), L16611, doi:10.1029/2006gl026817.

Hu, X., Q. Li, W.-J. Huang, B. Chen, W.-J. Cai, N. N. Rabalais, and R. E. Turner (2017), Effects of eutrophication and benthic respiration on water column carbonate chemistry in a traditional hypoxic zone in the Northern Gulf of Mexico, *Mar. Chem.*, 33–42, doi:10.1016/j.marchem.2017.04.004.

Huang, W.-J., W.-J. Cai, Y. Wang, S. E. Lohrenz, and M. C. Murrell (2015), The carbon dioxide system on the Mississippi River-dominated continental shelf in the northern Gulf of Mexico: 1. Distribution and air-sea CO_2 flux, *J. Geophys. Res. Ocean.*, *120*(3), 1429–1445, doi:10.1002/2014JC010498.

Hunt, C. W., J. E. Salisbury, and D. Vandemark (2014), CO_2 input dynamics and air-sea exchange in a large New England estuary, *Estuaries and Coasts*, *37*(5), 1078–1091, doi:10.1007/s12237-013-9749-2.

Jiang, L.-Q., W.-J. Cai, Y. Wang, R. Wanninkhof, and H. Lüger (2008), Air-sea CO_2 fluxes on the U.S. South Atlantic Bight: Spatial and seasonal variability, *J. Geophys. Res.*, *113*, C07019, doi:10.1029/2007jc004366.

Joesoef, A., W.-J. Huang, Y. Gao, and W.-J. Cai (2015), Air–water fluxes and sources of carbon dioxide in the Delaware Estuary: spatial and seasonal variability, *Biogeosciences*, *12*, 6085–6101, doi:10.5194/bg-12-6085-2015.

Kemp, W. M., P. A. Sampou, J. Garber, J. Tuttle, and W. R. Boynton (1992), Seasonal depletion of oxygen from bottom waters of Chesapeake Bay: Roles of benthic and planktonic respiration and physical exchange processes, *Mar. Ecol. Prog. Ser.*, *85*(1–2), 137–152, doi:10.3354/meps085137.

Kemp, W. M. et al. (2005), Eutrophication of Chesapeake Bay: Historical trends and ecological interactions, *Mar. Ecol. Prog. Ser.*, *303*, 1–29.

Lachkar, Z. (2014), Effects of upwelling increase on ocean acidification in the California and Canary Current systems, *Geophys. Res. Lett.*, *41*(1), 90–95, doi:10.1002/2013GL058726.

Lacy, J. R., M. T. Stacey, J. R. Burau, and S. G. Monismith (2003), Interaction of lateral baroclinic forcing and turbulence in an estuary, *J. Geophys. Res.*, *108*(C3), 3089, doi:10.1029/2002JC001392.

Lee, Y. J., W. R.Boynton, M.Li, andY.Li (2013), Role of Late Winter-Spring Wind Influencing Summer Hypoxia in Chesapeake Bay, *Estuaries and Coasts*, *36*(4), 683–696, doi:10.1007/s12237-013-9592-5.

Li, Y., and M. Li (2012), Wind-driven lateral circulation in a stratified estuary and its effects on the along-channel flow, *J. Geophys. Res. Ocean.*, *117*(9), doi:10.1029/2011JC007829.

Malone, T., W. Kemp, H. Ducklow, W. Boynton, J. Tuttle, and R. Jonas (1986), Lateral variation in the production and fate of phytoplankton in a partially stratified estuary , *Mar. Ecol. Prog. Ser.*, *32*, 149–160.

Malone, T. C. (1992), Effects of water column processes on dissolved oxygen, nutrients, phytoplankton and zooplankton, in *Oxygen dynamics in the Chesapeake Bay: A synthesis of recent research*, edited by D. E.Smith, M.Leffler, and G. Mackiernan, pp. 61–112, Maryland Sea Grant College, College Park, MD.

Raymond, P. A., J. E. Bauer, and J. J. Cole (2000), Atmospheric CO_2 evasion, dissolved inorganic carbon production, and net heterotrophy in the York River estuary, *Limnol. Oceanogr.*, *45*(8), 1707–1717, doi:10.4319/lo.2000.45.8.1707.

Sanford, L. P., K. G. Sellner, and D. L. Breitburg (1990), Covariability of dissolved oxygen with physical processes in the summertime Chesapeake Bay, *J. Mar. Res.*, *48*(3), 567–590, doi:10.1357/002224090784984713.

Scully, M. E. (2010), Wind modulation of dissolved oxygen in Chesapeake Bay, *Estuaries and Coasts*, *33*(5), 1164–1175, doi:10.1007/s12237-010-9319-9.

Scully, M. E. (2016), Mixing of dissolved oxygen in Chesapeake Bay driven by the interaction between wind-driven circulation and estuarine bathymetry, *J. Geophys. Res. Ocean.*, *121*(8), 5639–5654, doi:10.1002/2016JC011924.

Son, S., M. Wang, and L. W. Harding (2014), Satellite-measured net primary production in the Chesapeake bay, *Remote Sens. Environ.*, *144*, 109–119, doi:10.1016/j.rse.2014.01.018.

Takahashi, T. et al. (2002), Global sea-air CO_2 flux based on climatological surface ocean pCO_2, and seasonal biological and temperature effects, *Deep Sea Res. Part II Top. Stud. Oceanogr.*, *49*(9–10), 1601–1622.

Testa, J. M., and W. M. Kemp (2008), Variability of biogeochemical processes and physical transport in a partially stratified estuary : a box-modeling analysis, *Mar. Ecol. Prog. Ser.*, *356*, 63–79, doi:10.3354/meps07264.

Wanninkhof, R. (1992), Relationship between wind speed and gas exchange over the ocean, *J. Geophys. Res.*, *97*(C5), 7373–7382.

Wilson, R. E., R. L. Swanson, and H. A. Crowley (2008), Perspectives on long-term variations in hypoxic conditions in western Long Island Sound, *J. Geophys. Res.*, *113*(C12), C12011, doi:10.1029/2007JC004693.

Weiss, R. F. (1974), Carbon dioxide in water and seawater: the solubility of a non-ideal gas, *Mar. Chem.*, *2*(3), 203–215.

Xie, X., M. Li, and W. C. Boicourt (2017a), Baroclinic effects on wind-driven lateral circulation in Chesapeake Bay, *J. Phys. Oceanogr.*, (2014), JPO-D-15-0233.1, doi:10.1175/JPO-D-15-0233.1.

Xie, X., M. Li, and W. C. Boicourt (2017b), Breaking of internal solitary waves generated by an estuarine gravity current, *Geophys. Res. Lett.*, *44*(14), 7366–7373, doi:10.1002/2017GL073824.

Xie, X., M. Li, M. Scully, and W. C. Boicourt (2017c), Generation of internal solitary waves by lateral circulation in a stratified Estuary, *J. Phys. Oceanogr.*, *47*(7), 1789–1797, doi:10.1175/JPO-D-16-0240.1.

Xie, X. and M. Li (2018). Effects of wind straining on estuarine stratification: A combined observational and modeling study. J. *Geophys. Res. Ocean.*, 123, 2363–2380. https://doi.org/10.1002/2017JC013470

Zhai, W., M. Dai, W.-J. Cai, Y. Wang, and Z.Wang (2005), High partial pressure of CO_2 and its maintaining mechanism in a subtropical estuary: the Pearl River estuary, China, *Mar. Chem.*, *93*(1), 21–32.

Figure Captions

Figure 1. The study site, wind speed vector, and cross-channel variations in temperature, salinity, pCO_2, and CO_2 fluxes in the middle part of the Chesapeake Bay. (a) Geographic location of the study site where the ship surveys (black dots) were conducted and mooring arrays (gray triangles) were deployed. (b) Time series of wind speed vectors during October 24-25, 2013. The initial time and sequence of each circuit (D1 to D10) are labeled as vertical lines in the panel. The five white vertical bars indicate the mooring locations where salinity and temperature (c-f) were measured. (c) Depth-lateral distributions of salinity (colors) and lateral velocities (horizontal bars) displayed strong stratification during the D1. Upwelling to the eastern shoal was observed from D3 (d), became strong on D5 (e) and became relaxed on D10 (f). The binned averages of temperature, salinity, pCO_2, and air-sea CO_2 flux (and its standard deviation) in 0.008° of longitude are shown as open circles (and bars), displaying larger variations on the eastern shoal (g to j). The average atmospheric pCO_2 value was 400.9 ± 2.1 μatm. The stratification condition D1 (pink circle) displayed varied values in each panel compared with the upwelling condition D5 (blue triangle). In (g) to (j), all data are displayed as gray dots; the vertical gray dashed lines separate the western, middle, and eastern sections across the estuary.

Figure 2. Distributions of pCO_2 in each successful survey from D1 to D10. The D8 survey was interrupted by the failure of other equipment on board. We only have a few data across the estuary during D8, and thus D8 data were not displayed.

Figure 3. The relationship between bin-averaged pCO_2 (or binned air-sea CO_2 flux) and bin-averaged salinity, and the relationship between pCO_2 (or salinity) and wind speed (m s^{-1}). The strong correlation between pCO_2 and salinity was consistent with the idea that this surface pCO_2 variation was caused by upwelling through a counterclockwise circulation (a). pCO_2 values were better correlated with wind speed during the setup phase than the set-down phase (b).

Figure 4. The simulation of river to sea mixing and the simulation of mixing between brackish water and respired near-bottom water. The end-members are in Table S1.

Figure 5. The relationship between ln(pCO_2) and temperature. The slope shows the theoretical relationship between pCO_2 and temperature.

Figure 6. A conceptual model for wind-driven lateral circulation and the corresponding biogeochemical processes in a stratified estuary. During down-estuary winds, pCO_2 was high on the eastern shoal due to a counterclockwise circulation (a). During up-estuary winds, pCO_2 was high on the western shoal due to a clockwise circulation (b). Both down-estuary and up-estuary winds can produce conditions favorable for releasing respired DIC in the water column.

Table 1. Surface water pCO_2 and air-sea CO_2 flux on the western shoal (W), middle of the bay (M), and the eastern shoal (E). (Unit: pCO_2, μatm; CO_2 flux, mmol m^{-2} d^{-1}). The max wind during D5 was 7.0 m s^{-1}. The changes of values between in the shoals (W or E) and in the middle (M) were calculated. The differences of pCO_2 and CO_2 flux between in D5 and the average of D1 to D10 were also presented in the last two columns.

	Average		D5 (Max. wind)		Difference (D5 - Ave.)/Ave.	
	pCO_2	CO_2 flux	pCO_2	CO_2 flux	pCO_2	CO_2 flux
Western shoal (W)	450.0	7.6	445.2	6.8	-1%	-11%
(W – M)/M	(-2%)	(-22%)	(-6%)	(-46%)	-	-
Middle (M)	460.2	9.8	474.5	12.4	3%	27%
Eastern shoal (E)	483.9	13.3	516.4	19.0	7%	44%
(E – M)/M	(5%)	(30%)	(9%)	(53%)	-	-

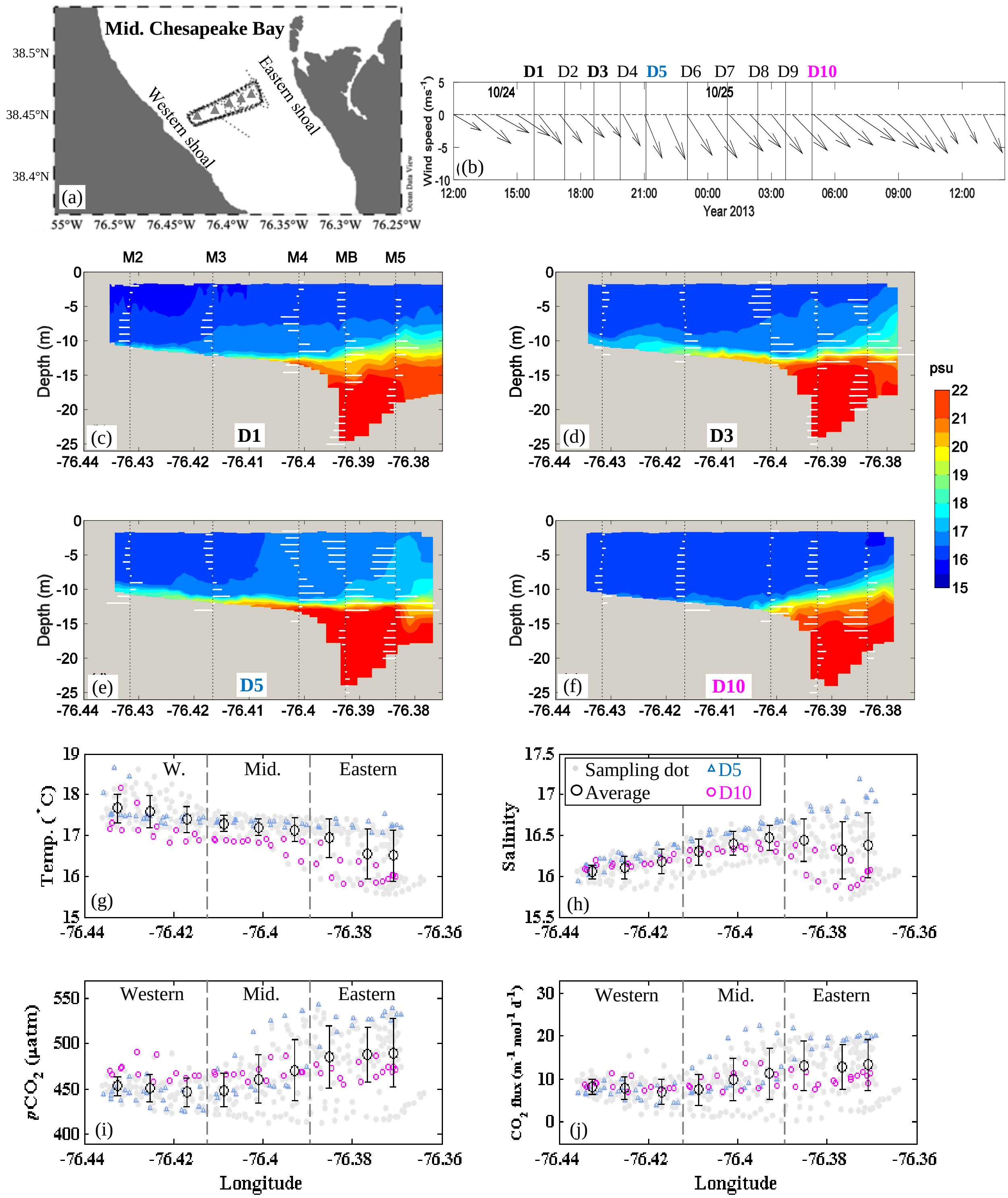
Mid. Chesapeake Bay
Western shoal
Eastern shoal
(a)
(b)
Wind speed (ms^{-1})
D1 D2 D3 D4 D5 D6 D7 D8 D9 D10
10/24
10/25
Year 2013
M2 M3 M4 MB M5
Depth (m)
psu
(c) D1
(d) D3
(e) D5
(f) D10
W. Mid. Eastern
Temp. (°C)
(g)
Salinity
(h)
Sampling dot
Average
D5
D10
Western Mid. Eastern
pCO$_2$ (μatm)
(i)
CO$_2$ flux (m^{-1} mol^{-1} d^{-1})
(j)
Longitude

Figure 1

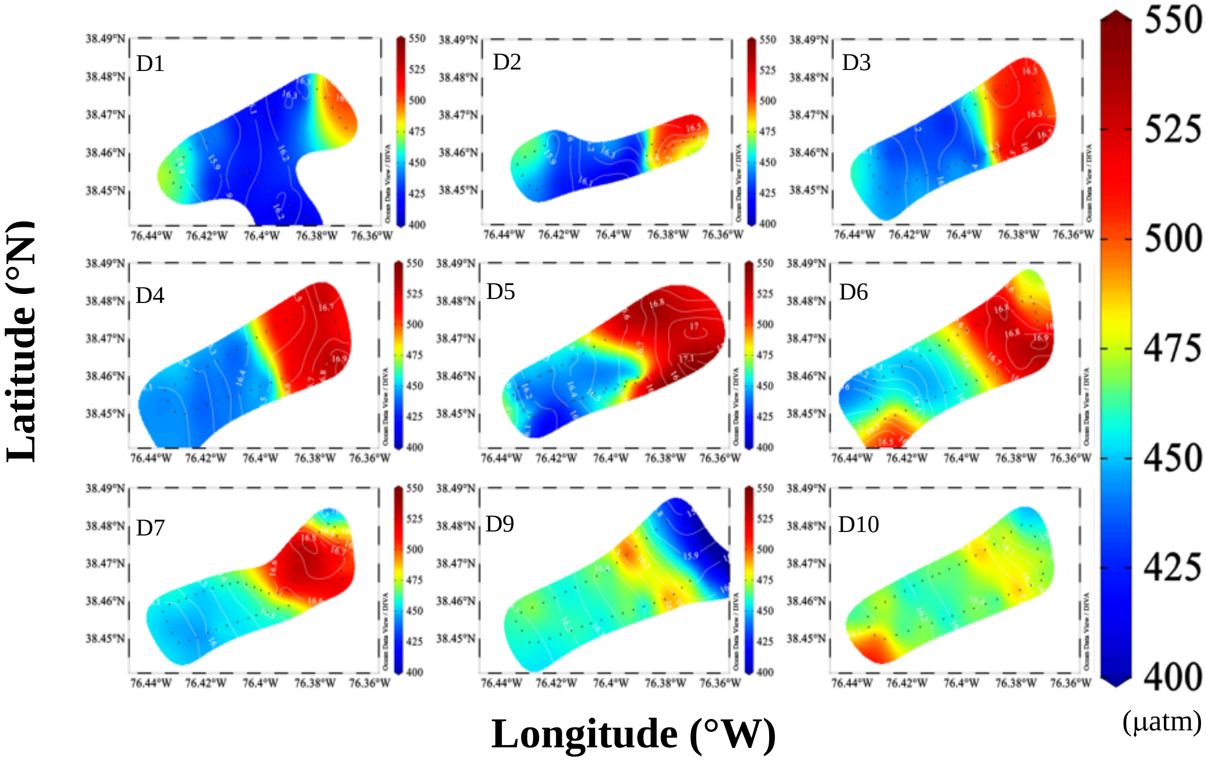
D1
D2
D3
D4
D5
D6
D7
D9
D10
Latitude (°N)
Longitude (°W)
550
525
500
475
450
425
400
(µatm)

Figure 2.

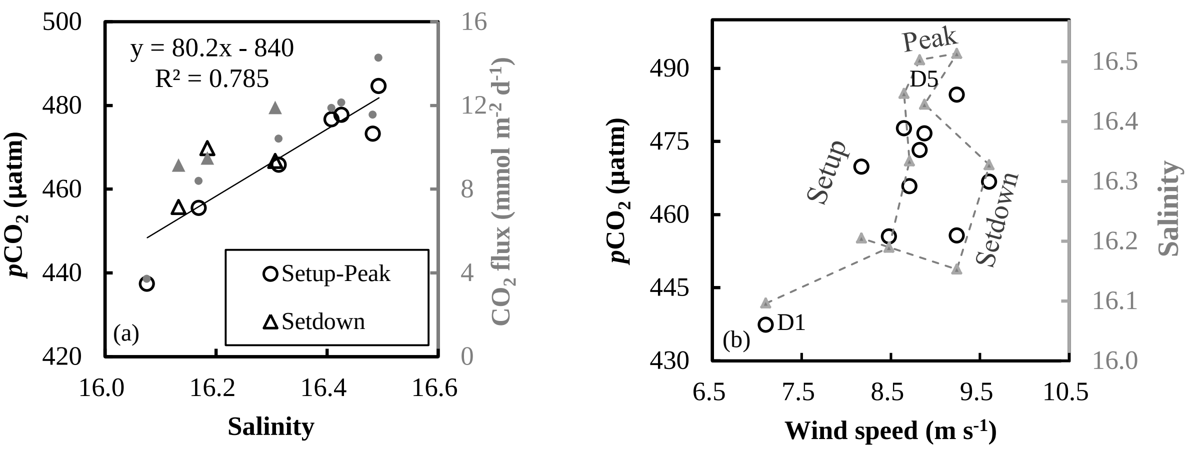

y = 80.2x - 840
R² = 0.785
Setup-Peak
Setdown
(a)
pCO2 (µatm)
CO2 flux (mmol m-2 d-1)
Salinity
500
480
460
440
420
16
12
8
4
0
16.0
16.2
16.4
16.6
Peak
D5
Setup
Setdown
D1
(b)
pCO2 (µatm)
Salinity
Wind speed (m s-1)
490
475
460
445
430
16.5
16.4
16.3
16.2
16.1
16.0
6.5
7.5
8.5
9.5
10.5

Figure 3

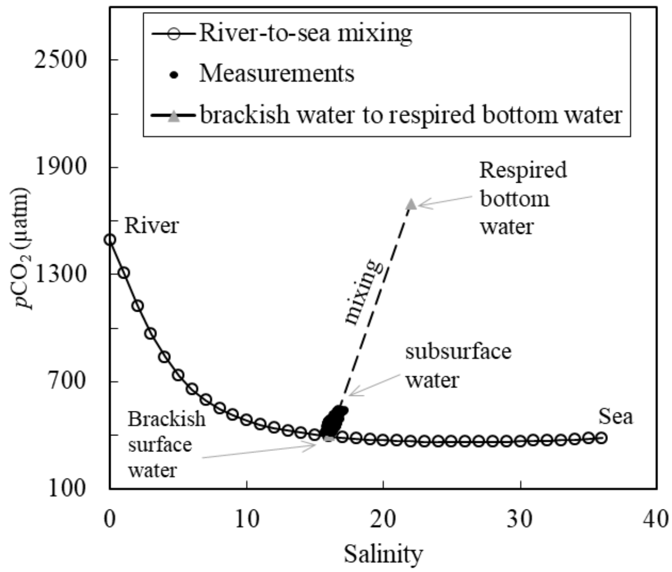
River-to-sea mixing
Measurements
brackish water to respired bottom water
Respired bottom water
River
mixing
subsurface water
Brackish surface water
Sea
pCO$_2$ (µatm)
2500
1900
1300
700
100
0
10
20
30
40
Salinity

Figure 4.

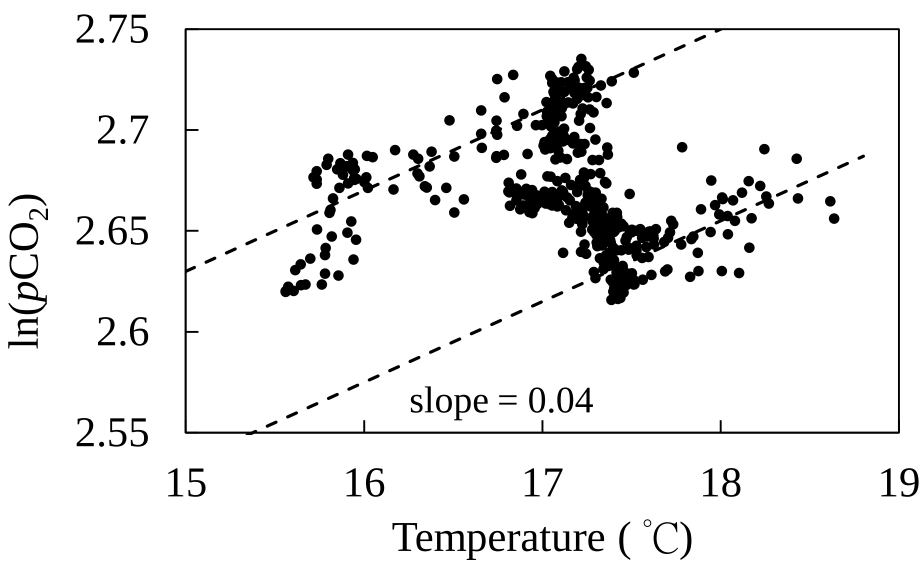

Figure 5.

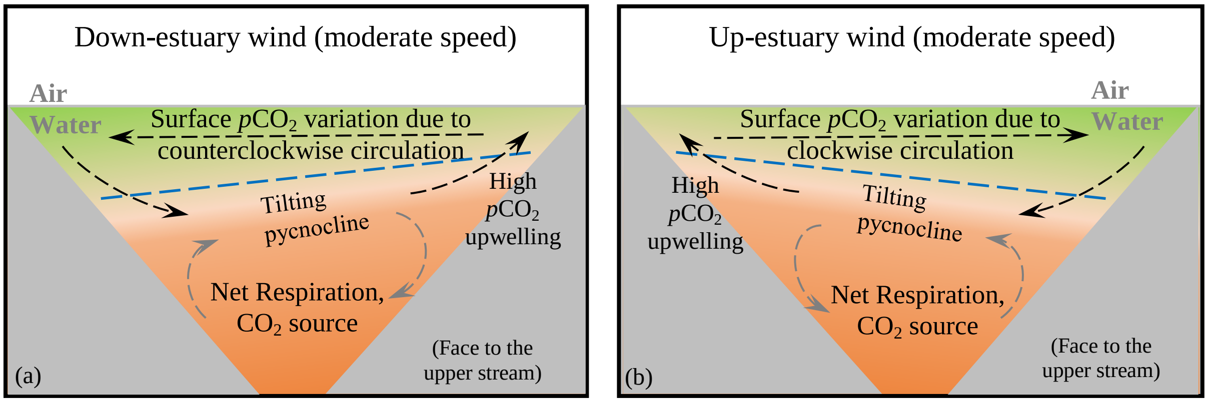

Down-estuary wind (moderate speed)
Air
Water
Surface pCO_2 variation due to counterclockwise circulation
Tilting pycnocline
High pCO_2 upwelling
Net Respiration, CO_2 source
(Face to the upper stream)
(a)
Up-estuary wind (moderate speed)
Air
Water
Surface pCO_2 variation due to clockwise circulation
High pCO_2 upwelling
Tilting pycnocline
Net Respiration, CO_2 source
(Face to the upper stream)
(b)

Figure 6